

Characteristics and catalytic behavior of supported NiMgAg/D catalysts in the partial hydrogenation of soybean oil

Miroslav Stanković · Željko Čupić ·
Margarita Gabrovska · Predrag Banković ·
Dimitrinka Nikolova · Dušan Jovanović

Received: 21 October 2014 / Accepted: 29 December 2014 / Published online: 15 January 2015
© Akadémiai Kiadó, Budapest, Hungary 2015

Abstract Diatomite supported NiMgAg catalysts, NiMgAg/D, were prepared by the precipitation-deposition method followed by drying, reduction and passivation. The preparation of the catalysts was performed with different loading of silver ranging from 0.16 to 5.88 wt% and constant molar ratios of SiO₂/Ni and Mg/Ni equal to 1.07 and 0.1, respectively. The characterization of the catalysts was performed with N₂-physisorption, mercury intrusion porosimetry, H₂-chemisorption, X-ray diffraction, temperature programmed reduction, and scanning electron microscopy-energy dispersive X-ray analysis. The partial hydrogenation of soybean oil from initial to final iodine value of 90 was carried out at 160 °C and H₂ pressure of 0.16 MPa using stirred semi-batch reactor. Soybean oil was hydrogenated over NiMgAg/D catalysts and NiMg/D catalyst (without silver addition) that was prepared using the same procedure as used for catalysts modified with silver. The selectivity towards *trans* fatty acid and saturated fatty acid formation was determined for both types of catalysts. By comparing the selectivity of the NiMgAg/D catalysts with the NiMg/D catalyst the promoting effect of silver modifier on the catalyst behavior in the hydrogenation of soybean oil was observed, and correlated with changing of the catalyst surface characteristics caused by the different Ag loading. It was found that the addition of silver to NiMg/D catalyst decreased both the selectivity towards *trans* fatty acids formation and the selectivity towards saturated fatty acids. For the same iodine value decay, the catalyst with the highest Ag loading (5.88 wt%) had the lowest level of both *trans* fatty acids and saturated fatty acids in the hydrogenation of soybean oil under studied operating conditions. The

M. Stanković (✉) · Ž. Čupić · P. Banković · D. Jovanović
Center of Catalysis and Chemical Engineering, University of Belgrade-Institute of Chemistry,
Technology and Metallurgy, Njegoševa 12, Belgrade, Republic of Serbia
e-mail: mikastan@nanosys.ihtm.bg.ac.rs

M. Gabrovska · D. Nikolova
Institute of Catalysis, Bulgarian Academy of Sciences, Acad. G. Bonchev Str., bl. 11, 1113 Sofia,
Bulgaria

hydrogenation activity of NiMgAg/D catalysts is lower than NiMg/D catalyst and decreases with increasing Ag loading. The correlation between adsorption characteristics of the catalysts and their hydrogenation activities was established. The proposed simplified kinetic model to describe the kinetics of soybean oil hydrogenation gave a good description of the experimental data.

Keywords Hydrogenation · NiMgAg/D catalyst · Activity · *Cis–trans* isomerization

Introduction

Catalytic hydrogenation of vegetable oils is an important process in the modification of fats and oils. The purpose of the partial hydrogenation of vegetable oil is to obtain a more stable product with a suitable texture and melting temperature for use as margarine and edible shortenings. The catalytic slurry batch process is customary in the vegetable oil hydrogenation industry with nickel (Raney or supported) catalyst, at high temperatures, low pressures and long reaction times [1]. The effects of process parameters such as temperature, hydrogen pressure, catalyst loading and stirring rate on the activity and selectivity, and *trans* fatty acids (TFA) formation are reported in the literature [2–6].

Besides the process conditions, the catalyst formulation is an important factor contributing to the TFA and saturated fatty acids (SFA) formation during hydrogenation. As an unavoidable side reaction occurring during the catalytic hydrogenation, the geometric isomerization producing TFA can be influenced by the choice of dispersed metal on the solid support and its surface characteristics. Therefore, it is desirable to design catalysts with tailored characteristics, offering higher selectivity towards products with *cis* configuration, and lower selectivity towards saturated product formation. The activity, selectivity and stability of nickel catalysts, supported or Raney-nickel, are known to be greatly influenced by their chemical and phase composition, type of crystal aggregation and dispersity [7].

In the last three decades, a numerous research works were published in order to know the effect TFA on the cellular metabolism. TFA intake has been convincingly associated with risk of heart disease based on epidemiologic and clinical studies, and has been shown to be harmful to human health [8, 9]. For this reason, the demand for smaller levels of TFA content in hydrogenated oils has increased, and the search of alternatives is important to improve the hydrogenation process. A field in which there have been major advances is that of hydrogenation catalysts [10–15]. The bulky size of the triglyceride molecules, together with the simultaneity of other reactions, as those of geometric or positional isomerization, can imply that the reaction could be sensitive to catalyst structure.

Research aimed at understanding the role of modifiers and/or promoters on activity and selectivity of catalyst is quite scarce in the literature. The effect of modifiers and/or promoters appears to depend on the nature of promoter and/or modifier, and of the methods of preparation, activation and reduction of catalysts [10, 13, 16–18].

Summarizing the literature, it could be concluded that the following factors should be considered while developing active and selective supported metal catalyst for hydrogenation of vegetable oils: (1) high dispersion of active metal and resistance to sintering; (2) active metal accessibility for the reactant (triglycerides) molecules; (3) oil-catalyst interactions.

Several kinetic models of the hydrogenation of fatty oils containing polyunsaturated fatty acids were devised previously, and reaction rate constants were evaluated for the various reactions [19–22]. All of the proposed reaction schemes were incomplete. From a practical standpoint, it is justified because of the extreme complexity of the complete kinetic model, which would have to include all possible consecutive and isomerization reactions.

The scope of this study, based on a preliminary investigation [13], is to correlate the surface characteristics of NiMgAg/D catalysts with their catalytic behavior in the hydrogenation of soybean oil. The effect of Ag loading on the reduction ability and on the activity and selectivity towards TFA formation is emphasized. A comparative evaluation of the NiMgAg/D catalysts with silver modifier and NiMg/D catalyst in the hydrogenation of soybean oil is carried out. The kinetics of soybean oil hydrogenation is described by a simplified kinetic model. The specific goal of the present study was to extend the preliminary investigation [13] by more thorough characterization, expected to provide more information on the synthesized catalysts and the catalytic process itself. In addition, a simplified reaction model will be established and compared with the experimental data, and corresponding kinetic parameters will be calculated.

Experimental

Catalyst preparation

Catalysts were prepared according to procedures described previously [23]. A short description will be given here. Crude diatomite material was supplied from Baroševac—field B “Kolubara” coal basin, Lazarevac, Serbia. Prior to precipitation, the crude material was mechanically, chemically and thermally treated to obtain the desired support characteristics. The diatomite support (D) obtained after activation had the following textural characteristics: surface area of $29 \text{ m}^2 \text{ g}^{-1}$ (S_{BET} , N_2 -physisorption), intrusion pore volume of $1.403 \text{ cm}^3 \text{ g}^{-1}$, the average pore diameter of 465 nm and total porosity of 73 % (MIP).

NiMgAg/D catalyst precursors with different Ag loading were prepared by precipitation-deposition method. The precipitation of Ni, Mg and Ag was performed by addition of anhydrous sodium carbonate to a solution containing Ni, Mg and Ag nitrate salts. The deposition of precipitates onto the diatomite support was carried out by adding a hot aqueous suspension of diatomite to a slurry containing precipitates of corresponding metals. For the preparation of the NiMg/D catalyst precursor, the same procedure was used excluding the addition of the Ag salt. Afterwards, the precursors were aged, filtered, washed, dried at $110 \text{ }^\circ\text{C}$ overnight, and finally activated by reduction with a gas mixture of H_2/N_2 (1/1, v/v) in an oven

at 430 °C for 5 h at the heating rate of 1.5 °C min⁻¹. A part of the activated precursor sample was passivated (350 ppm of O₂ in nitrogen) for characterization and handling.

The NiMgAg/D catalysts prepared with the silver loadings 0.16, 1.55 and 5.88 wt%, hereafter referred to as NiMgAg(0.16)/D, NiMgAg(1.55)/D and NiMgAg(5.88)/D. Likewise, the catalyst prepared without silver addition, hereafter referred to as NiMg/D.

Characterization techniques

Inductively coupled plasma–optical emission spectroscopy (ICP–OES)

The chemical composition of the support and Ni, Mg and Ag loadings in the studied samples was measured by ICP–OES on an iCAP 6500 Duo apparatus manufactured by Thermo Fisher Scientific. Before analysis, the samples were subjected to microwave digestion using a Milestone Ethos 1 advanced microwave digestion system.

Determination of textural characteristics

The specific surface area of the support and the reduced-passivated catalyst precursors were determined by nitrogen physisorption at liquid nitrogen temperature according to the BET method. A surface area of 0.162 nm² for the physically adsorbed N₂ molecule was used for calculation of the BET surface area. Measurements were carried out by static physisorption with an automatic physisorption apparatus (Sorptomatic 1990, Thermo Finnigan). Samples were outgassed at 110 °C for 16 h prior to the measurements. The mesopore volume (V_{meso}) and micropore volume (V_{micro}) of the samples were calculated using BJH algorithm and Dubinin and Raduskevich method. Mercury intrusion porosimetry (MIP) measurements were performed in a Porosimeter 2000 equipped with the Macropore unit 120 (Carlo Erba Instruments).

Powder X-ray diffraction (XRD)

Powder XRD was carried out in a Phillips powder diffractometer mounted on a Philips PW1710 X-ray generator using the K_α radiation of Cu ($\lambda = 0.154178$ nm).

Hydrogen chemisorption

H₂ chemisorption at 25 °C was used to determine the nickel crystallite size and nickel surface area. The measurements were performed by the static method in a standard volumetric apparatus. The monolayer adsorption capacity was determined by extrapolation down to zero pressure with the linear regression of the equilibrium data in the range 0.1–13.3 kPa. Chemisorption measurements were carried out under the following conditions: in situ reduction of precursor samples under a H₂/N₂ (1/1, v/v) gas mixture stream at 430 °C and the heating rate of 2 °C min⁻¹. A

detailed description of the experimental procedure and discussion concerning its adequacy was provided elsewhere [24–27].

The nickel surface area was calculated with the following equation:

$$S_{Ni}(m_{Ni}^2 g_{Ni}^{-1}) = 1.298 \times 10^{-19} N_M \quad (1)$$

Here, N_M is the number of hydrogen molecules adsorbed in the monolayer per gram of nickel. Equation 1 was derived considering the surface occupied per atom of nickel as $6.33 \times 10^{-2} \text{ nm}^2 \text{ atom}^{-1}$ [28], and the adsorption stoichiometry as 0.5 hydrogen molecules per surface nickel atom.

The average size of the nickel crystallites (d_{sNi}) in the sample was calculated assuming a model in which hemispherical crystallites are attached to the support with their equatorial plane. For this model the crystallite size (defined as the cube root of the volume) was calculated from the nickel area per gram of nickel (S_{Ni}) using the expression [28]:

$$d_{sNi}(nm) = 431/S_{Ni} \quad (2)$$

Temperature programmed reduction (TPR)

Reduction experiments were performed in an atmospheric plug-flow reactor using thermal conductivity detector to monitor the hydrogen consumption. A fractured precursor sample (0.50–0.70 mm) was reduced in a $25 \text{ cm}^3 \text{ min}^{-1}$ of 1/9 (v/v) H_2/Ar gas flow, while the temperature was changed from 100 to 900 °C at a linear heating rate of $10 \text{ }^\circ\text{C min}^{-1}$.

Scanning electron microscopy-energy dispersive X-ray (SEM-EDX)

Electron microscopic measurements and energy-dispersive element analysis were performed in a JEOL Superprobe 733 scanning electron microscope equipped with a Link AN10000 EDX system for quantitative elemental analysis.

Catalyst testing

The catalyst activity was tested in the partial hydrogenation of soybean oil. The experiments were carried out in a pilot-plant semi-batch reactor (7.5 dm^3), in which the reactant oil and catalyst were fed at the beginning of the experiment, and hydrogen was continuously bubbled in the oil. The catalytic tests were performed at temperature of 160 °C, H_2 pressure of 0.16 MPa and stirring rate of 750 rpm. The course of the reaction was followed by analysis of liquid samples taken out at intervals. The composition of original soybean oil and hydrogenated products was analyzed by gas chromatography (GC) using a 100 m HP-88 capillary column (Agilent). The injection port and column were maintained at 240 °C and 180 °C, respectively, and split injection was used in a 1:4 split ratio. Before the analysis, samples obtained from the catalytic reactor were converted into their corresponding methyl esters according to IUPAC method II.D.19 [29].

Results and discussion

Catalyst metal loading and chemical composition of diatomite support

Table 1 lists the designation of prepared catalysts, metal loadings of catalysts, and chemical composition of diatomite support.

X-ray diffraction

The XRD results of the reduced-passivated catalyst precursors are shown in Fig. 1. Diffractogram of the NiMg/D sample shows that a crystalline metallic nickel is formed upon reduction at 430 °C. The main diffraction peaks, which adjust with the JCPDS 04-0850 pattern, correspond to cubic Ni, at 2θ values of 44.62, 51.91 and 76.33. The great similarity between the diffractograms of the NiMg/D sample and the sample with the lowest Ag loading, NiMgAg(0.16)/D, is indicative for the high dispersion of metallic silver in the sample.

The diffractograms of samples with Ag loadings of 1.55 and 5.88 wt% show a higher degree of crystallinity, which is clearly evident in the diffraction pattern of the sample with the highest Ag loading. The four diffraction peaks obtained at angles 2θ of 38.13, 44.29, 64.46 and 77.38, respectively, are attributed to the face centered cubic crystalline silver (JCPDS 4-0783). It must be pointed out that the peak of the highest intensity for metallic nickel overlaps very intense peak of metallic silver at angle 2θ of 44.29. The size of silver crystallites calculated from line broadening using the Scherrer equation [30, 31] range from 22 to 29 nm for the NiMgAg(5.88)/D sample.

Catalyst texture

In order to obtain textural parameters including specific surface area and pore volume in meso- and microscale pore sizes, N₂ adsorption–desorption isotherms were measured at liquid nitrogen temperature (−196 °C). Fig. 2 compares the isotherm curves for the diatomite support and reduced-passivated catalyst precursors. On the basis of Brunauer, Deming, Deming and Teller classification [32], the adsorption–desorption isotherms for diatomite belong to a typical type II, indicating that the support should be macroporous powder or powder with pore diameters larger than micropores [33].

It is obvious that the adsorption–desorption isotherms of the support and of the reduced-passivated catalyst precursors are quite different. A distinct increase in nitrogen volume in the low relative pressure region indicates the presence of micropores associated with mesopores. The amount of nitrogen adsorbed increases gradually and hysteresis loops are observed when $p/p_0 > 0.42$, indicating the existence of many meso- and macropores in the catalysts. The obtained isotherms of the reduced-passivated catalyst precursors are very similar in shape and typical for well-defined mesoporous frameworks. In general, catalysts of the “mesoporous group” produced isotherms with desorption branch that met with the adsorption branch at $p/p_0 = \sim 0.45$ – 0.50 and the two branches coincided at lower pressure

Table 1 Designation and metal loadings of prepared catalysts

Catalyst designation	Ni loading (wt%)	Mg loading (wt%)	Mg/Ni (molar ratio)	Ag loading (wt%)			
NiMg/D	39.89	1.65	0.10	–			
NiMgAg(0.16)/D	35.94	1.49	0.10	0.16			
NiMgAg(1.55)/D	35.16	1.45	0.10	1.55			
NiMgAg(5.88)/D	33.51	1.39	0.10	5.88			
Chemical composition of diatomite support							
Diatomite support	SiO ₂ (wt%)	Al ₂ O ₃ (wt%)	MgO (wt%)	CaO (wt%)	Fe ₂ O ₃ (wt%)	K ₂ O (wt%)	Na ₂ O (wt%)
	93.47	3.94	0.88	0.59	0.56	0.57	0.06

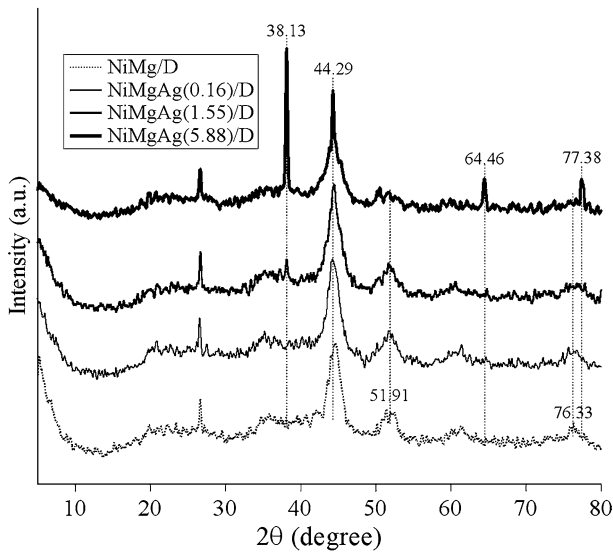


Fig. 1 XRD diffractograms of NiMg/D, NiMgAg(0.16)/D, NiMgAg(1.55)/D and NiMgAg(5.88)/D of reduced-passivated catalyst precursors

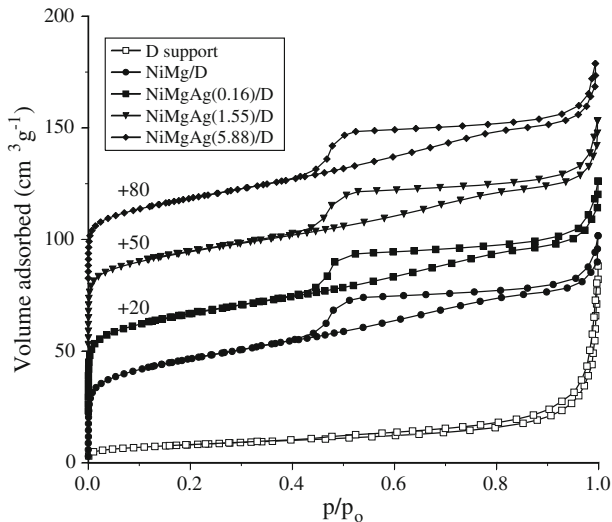


Fig. 2 Adsorption–desorption isotherms of diatomite support and reduced-passivated catalyst precursors

points. The isotherms of the reduced-passivated catalyst precursors cannot be classified as typical although they mostly resemble type II according to IUPAC classification. Table 2 summarizes the textural characteristics of reduced-passivated catalyst samples.

Table 2 Textural parameters of studied samples (N₂ physisorption)

Sample	S _{BET} ^a (m ² g ⁻¹)	S _{meso} ^b (m ² g ⁻¹)	V _{meso} ^c (cm ³ g ⁻¹)	V _{micro} ^d (cm ³ g ⁻¹)	V _{total} ^e (cm ³ g ⁻¹)
NiMg/D	164	94 ^a	0.093 ^a	0.065 ^a	0.158
NiMgAg(0.16)/D	163	93 ^a	0.093 ^a	0.066 ^a	0.159
NiMgAg(1.55)/D	157	92 ^a	0.094 ^a	0.063 ^a	0.157
NiMgAg(5.88)/D	136	102 ^a	0.104 ^a	0.053 ^a	0.157

^a BET surface area^b Mesopore surface area (BJH method)^c Mesopore volume (BJH method, desorption branch)^d Micropore volume (Dubinin Raduskevich method)^e Total pore volume at $p/p_0 = 0.98$

The specific surface areas and pore structures of the NiMgAg/D samples with loadings up to 1.55 wt% (NiMgAg(0.16)/D and NiMgAg(1.55)/D) are similar to the textural parameters measured for the NiMg/D sample. However at the highest Ag loading the micropore volume of the sample NiMgAg(5.88)/D is reduced (Table 2). The prepared samples have BET surface areas, which are an order of magnitude larger than the surface area of the support. This was also observed by several authors [28, 34] in the case of Ni/diatomite or Ni/SiO₂ catalysts prepared by precipitation-deposition method. An extreme increase in BET surface area of the samples can be attributed to the formation of layered structure Ni compound developing a new surface area that is formed in the metal-support interaction [28, 35–37].

Hydrogen chemisorption

Isotherms obtained over the prepared precursor samples are shown in Fig. 3. The total hydrogen uptake was determined from zero pressure intercepts of the isotherms. The addition of Ag (hydrogen does not adsorb onto silver at 25 °C) to NiMg/D sample results in a large decrease of hydrogen adsorbed.

Chemisorption results of the precursor samples are listed in Table 3. The estimates of crystallite size from H₂ chemisorption are also compared in Table 3 with the values determined from X-ray diffraction methods line broadening (XRDLB).

Hydrogen chemisorption is commonly used as a suitable and reliable tool for the determination of the size of active metal surface area [38]. However, the active metal surface calculation is dependent on the stoichiometry of the hydrogen adsorption which in turn depends on the metal-support interaction, promoters and preparation method [39]. It should be emphasized that the estimation of metal crystallite size from hydrogen uptake requires the assumptions to be made regarding metal crystallite morphology. To calculate the average crystallite size, it was assumed hemispherical shape of nickel crystallites which is suitable for the supported catalysts with strong metal-support interaction. The average size of nickel

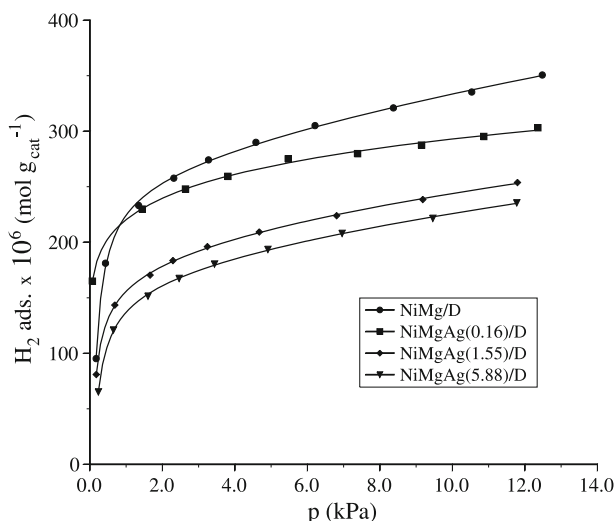


Fig. 3 Adsorption isotherms of catalyst precursors at 25 °C

Table 3 Hydrogen chemisorption results

Sample	H ₂ uptake ($\mu\text{mol g}_{\text{Ni}}^{-1}$)	S _{Ni} ^a ($\text{m}_{\text{Ni}}^2 \text{g}_{\text{Ni}}^{-1}$)	H ₂ chem d _{sNi} ^b (nm)	XRDLB d _{vNi} ^c (nm)
NiMg/D	744	58.2	7.4	7.1
NiMgAg(0.16)/D	709	55.4	7.8	8.3
NiMgAg(1.55)/D	538	42.1	10.2	11.7
NiMgAg(5.88)/D	513	40.2	10.7	13.6

^a Nickel surface area

^b Average size of Ni crystallites—surface-averaged values

^c The average size of Ni crystallites—volume-averaged values

crystallite of the studied samples deduced by static H₂ chemisorption method was confirmed by XRDLB method (Table 3). A large decrease in the nickel metal surface area of NiMgAg/D samples when compared to NiMg/D can be result of the following events: (a) nickel active site blocking by silver atoms, (b) electronic interactions between Ni and Ag atoms that affect the hydrogen binding to the surface Ni, and (c) changes in the stoichiometry of hydrogen adsorption on Ni surfaces due to structure sensitivity [40]. However, the agreement between results obtained with the different techniques led us to believe that no changes in H-Ni stoichiometry took place and to assume physical blocking of the nickel surface sites by silver atoms.

Temperature programmed reduction (TPR)

TPR profiles of the NiMgAg/D catalyst precursors are displayed in Fig. 4. For NiMg/D sample (not shown) the reduction profile was quite similar to the sample

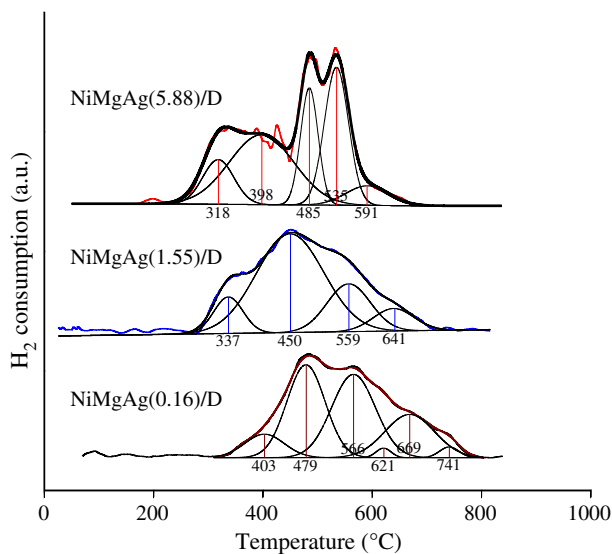


Fig. 4 Temperature programmed reduction profiles of NiMgAg/D catalyst precursors

with the lowest Ag loading (0.16 wt%) To attribute the reduction peaks to the transformation of corresponding metal phases by analyzing the reduction profiles only is difficult. It is more likely that a combination of effects is responsible for the complicated profiles. Although the individual processes proceedings cannot easily be assigned, the TPR results can be used as a fingerprint for comparing the studied samples.

TPR measurements clearly showed the differences in reducibility of NiMgAg/D samples. The reduction pattern of the NiMgAg(5.88)/D sample is characterized by onset of five peaks (Fig. 4). Generally, two separate regions of hydrogen consumption can be distinguished: (1) a low temperature region (LTR) from 210 to 440 °C (maxima of TPR peaks 318 and 398 °C) and (2) a high temperature region (HTR) from 440 up to 700 °C (maxima of TPR peaks 485, 535 and 591 °C). The hydrogen consumption at the LTR corresponds to easy reducible silver(I) and nickel(II) phases (Ag oxide or carbonate or Ni-basic carbonate). The higher TPR peak at LTR is in agreement with XRD, which also revealed the presence of more bulk-like silver upon increasing Ag loading (Fig. 1). Hydrogen consumption at HTR is normally attributed to hardly reducible Ni(II) phases (Ni phyllosilicates). It is well-known that the method of precipitation-deposition leads to the formation of supported 1:1 or 2:1 Ni phyllosilicates. These structures are well-known and were extensively described in the literature [37]. When the Ag loading is decreased, the reduction profiles become less resolved (NiMgAg(1.55)/D and NiMgAg(0.16)/D), which indicates that the reduction proceeds in a single unresolved step (Fig. 4). It is important to note that increasing Ag loading in the samples shifts the onset temperatures of the initial reduction to lower temperatures (Fig. 4). Furthermore, the reduction was completed at lower temperatures with the samples of higher Ag loadings.

Although the nickel particles of samples do not easily sinter because of the strong interaction with support [35–37], XRD and H_2 chemisorption results are shown that increasing the Ag loading led to larger nickel crystallites in the silver modified samples, NiMgAg/D, which displayed easier nickel reduction. The dependence of the nickel metal particle size on the catalyst reducibility is usually accepted in the literature: the lower reducibility, the smaller the nickel metal particles [41, 42]. This observation could be an explanation for the better reducibility of the samples with higher Ag loadings.

It is well-known that TPR is often used for studying the influence of promoter metals and support effects on a catalyst reduction ability of supported catalysts [43]. The effect of silver addition on the reduction ability of transition metals has not been thoroughly researched in the literature. Richardson and co-workers [44] pointed out the positive role of silver oxide in promoting reduction of nickel oxide. A more efficient reduction of nickel oxide in the presence of silver is explained by easier nucleation of the nickel clusters. In bimetallic catalysts, the higher the silver loading the deeper the reduction occurs. Reduced silver forms metal particles acting as foreign nuclei for subsequent growth and reduction of nickel particles. The more silver cations were introduced in the catalyst, the more silver nuclei formed for nickel particles growth and nickel was reduced.

Scanning electron microscopy-energy dispersive X-ray

SEM-EDX pictures of reduced-passivated catalyst precursors are presented in Fig. 5. The SEM pictures display well-pronounced habit. The surface consists of fragments different in shape and size. The larger ones have an effective diameter of 3–7 μm . These are covered with numerous fine particles.

Fig. 5 also shows the elemental map of samples. The distribution of elements observed by EDX is given for some of important elements present in the studied samples. It is likely that the distribution of Ag in the samples with lower Ag loading was more or less homogenous (Figs. 5b and c). In contrast, the elemental map of the sample with the highest Ag loading (5.88 wt%), indicates that Ag was not only present in the dispersed state, but also in the form of agglomerates (Fig. 5d). Due to the non-uniform distribution of silver, as well as the low resolution of the nickel and magnesium lines, the atomic concentration of the elements obtained by EDX can be taken only as approximate. Estimations of the atomic compositions of the samples by SEM-EDX are presented in Table 4.

The atomic percentages of most of the elements, except for silver in NiMgAg(5.88)/D sample, are smaller than their nominal values, which could be caused by their irregular distribution at the sample surface.

Hydrogenation of soybean oil

Rate of hydrogenation and hydrogenation activity

A comparative study of the soybean oil hydrogenation was done using silver modified NiMgAg/D catalysts and NiMg/D catalyst under the same reaction

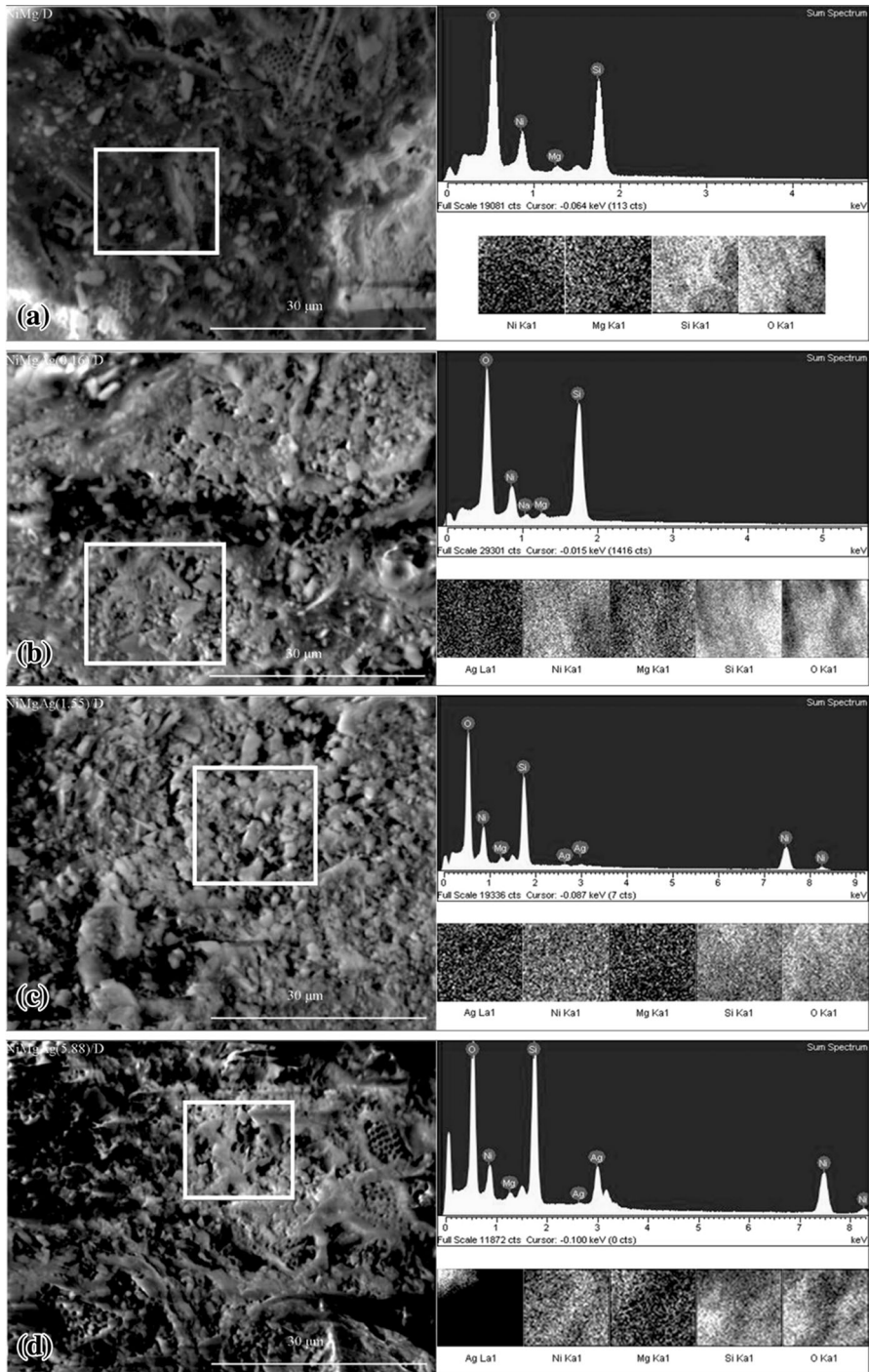


Fig. 5 SEM micrographs, EDX mapping and EDX spectra of reduced-passivated catalyst precursors

Table 4 SEM-EDX: Analyses of the atomic compositions

Sample	Concentration of element (at%) ^a				
	Ni (K)	Mg(K)	Ag (L)	Si(K)	O(K)
NiMg/D	2.27	1.29	–	11.85	84.59
NiMgAg(0.16)/D	4.07	1.04	<0.01	14.44	80.44
NiMgAg(1.55)/D	4.77	1.30	0.18	11.78	81.97
NiMgAg(5.88)/D	4.98	1.00	1.82	12.45	79.75

^a Normalized values**Table 5** Hydrogenation of soybean oil: Rate of hydrogenation and hydrogenation activity

Catalyst	Ni _{lccch} (g)	IV _f (g I ₂ 100 ⁻¹ g _{oil} ⁻¹)	t _{react} (min)	H _{2consum} (mol H ₂)	r _{hydr} ^b (mol H ₂ min ⁻¹)	A _{hydr} (mol H ₂ min ⁻¹ g ⁻¹ Ni)
NiMg/D	0.9972 ^a	89.3	75	8.018	0.107	0.107
NiMgAg(0.16)/D	0.8985 ^a	90.6	81	7.762	0.096	0.106
NiMgAg(1.55)/D	0.8790 ^a	90.0	155	7.880	0.051	0.058
NiMgAg(5.88)/D	0.8377 ^a	90.0	255	7.880	0.031	0.037

^a In catalyst charge (catalyst concentration of 0.05 wt%, *i.e.* 2.5 g catalyst/5,000 g oil) for hydrogenation run^b Rate of hydrogenation: $r = [(IV_0 - IV_f)/t_{\text{react}}] \cdot H_{2\text{consum}}$

conditions of temperature (160 °C), hydrogen pressure (0.16 MPa) and stirring rate (750 rpm), and iodine value (IV) decay of about 40. Hydrogenation activity was monitored by the decay of iodine value, which indicates the level of saturation of double C=C bonds. The IV measures the unsaturation of oil and fatty acids expressed in terms of the number of grams of iodine per 100 g of oil.

The rate of hydrogenation was measured from the hydrogen consumption at 160 °C and H₂ pressure of 0.16 MPa. The hydrogenation activity (A_{hydr}) was calculated from the following equation:

$$A_{\text{hydr}} = \frac{IV_0 - IV_f}{t_{\text{react}}} \cdot \frac{H_{2\text{consum}}}{Ni_{\text{lccch}}} \quad (3)$$

Here, IV₀ is the iodine value of the original soybean oil (130.0), IV_f the corresponding value of the hydrogenated oil, t_{react} the reaction time, H_{2consum} the hydrogen consumption for decay in iodine value of one unit and Ni_{lccch} the nickel loading in the catalyst charge for hydrogenation run.

Table 5 lists the rate of hydrogenation and hydrogenation activity of the catalysts. When comparing the results of catalyst testing in the hydrogenation reaction over NiMg/D catalyst and NiMgAg(0.16)/D catalyst, it can be observed that both catalysts are similarly active. The addition of silver inhibits hydrogenation activity, this effect being more obvious as the Ag loading is higher. The rate of hydrogenation and hydrogenation activity for the catalysts are given in Table 5 decreasing in the following order: NiMg/D ≥ NiMgAg(0.16)/D > NiMgAg(1.55)/D > NiMgAg(5.88)/D.

The large differences in the activity of the studied catalysts can be explained with their different adsorption characteristics. From the results obtained by N_2 physisorption and H_2 chemisorption, and the catalyst behavior in the hydrogenation reaction, the correlation between their adsorption properties and catalyst activities is obvious. The NiMg/D catalyst with the highest total surface area (BET) and the highest nickel surface area showed the highest activity. On the other hand, the NiMgAg(5.88)/D catalyst with the lowest both BET and nickel surface area had the lowest activity. This indicates that the role of both metal and total surface area is critical in assessing the catalytic efficiency.

For a typical hydrogenation of soybean oil with a 0.05 wt% Ni/SiO₂ commercial catalyst at 180 °C near atmospheric pressure, the rate of hydrogenation was found to be 0.0843 min⁻¹ corresponding to a catalyst activity of ~0.013 mol H₂ min⁻¹ g⁻¹ Ni [45]. In the present case, the catalyst activities of each studied catalysts are considerably higher than the commercial Ni/SiO₂ catalyst.

Cis–trans isomerization

The hydrogenation of soybean oil containing three-unsaturated linolenic acid (C18:3c) is a complex network of chemical reactions involving several reactant species. The overall hydrogenation reaction involves consecutive saturation of C18:3c to C18:2c, C18:2c to C18:1c, and subsequent saturation of C18:1c to C18:0 as well as parallel reversible isomerization of C18:2c to C18:2t and C18:1c to C18:1t. The reaction pathway may also involve a simple step hydrogenation of C18:1t to C18:0 and C18:2t to C18:1t.

The composition of the constituent fatty acids in original soybean oil and composition of hydrogenated soybean oil at conversion ($C = C_{\text{conv}}$) of 30.8 ± 0.5 are shown in Table 6. In all the cases, there was an increase in the concentration of stearic acid (C18:0) and a decrease in linoleic acid (C18:2c). It should be emphasized that linolenic acid (C18:3c) conversion after 30 min of reaction was 100 % on all catalyst studied. These results are expected having in mind that silver modified catalysts show high saturation selectivity toward linoleic acid formation [46].

As the present work is focused on the control of the TFA, the geometric isomers are presented in Table 6 without taking into account the position of double bond in the fatty acid chain, only distinguishing between *cis* fatty acids (CFA) and TFA.

Fig. 6 objectively shows the data summarized in Table 6. From these data, a comparison can be carried out among the studied catalysts. For almost the same level of conversion the NiMgAg(5.88)/D catalyst formed the least TFA of all catalysts (26.3 %). On the other hand, the NiMg/D catalyst showed the highest level of TFA (61.2 %), which could be related to its activity exhibited in the hydrogenation of soybean oil and more developed surface area compared to the catalysts modified with silver. It was reported that a large surface area favors isomerization reactions, due to the greater accessibility to the active sites [47].

The slight increase of stearic acid in the order: NiMg/D > NiMgAg(0.16)/D > NiMgAg(1.55)/D > NiMgAg(5.88)/D can be explained by the small differences observed in their textural characteristics (Table 2). According to Balakos and

Table 6 Hydrogenation of soybean oil: (%)

Fatty acids	Soybean oil	Catalyst			
		NiMgAg(0.16)/D	NiMgAg(1.55)/D	NiMgAg(5.88)/D	NiMg/D
C14:0	0.5	0.5	0.5	0.5	0.5
C16:0	11.1	11.1	11.1	11.1	11.1
C16:1	0.8	0.8	0.8	0.8	0.8
C18:0	4.5	8.1	6.2	5.8	8.6
C18:1 _c	21.3	18.7	22.5	22.7	15.9
C18:1 _t	–	49.1	16.5	10.8	53.1
C18:2 _c	53.8	1.2	22.7	31.7	0.9
C18:2 _t	–	1.4	2.5	2.0	1.7
C18:2 _{ct}	–	3.9	7.6	6.9	2.9
C18:2 _{tc}	–	4.2	8.3	6.6	3.5
C18:2 _t ^a	–	9.5	18.4	15.5	8.1
C18:3 _c	7.1	0.0	0.0	0.0	0.0
C20:0	0.3	0.3	0.3	0.3	0.3
C20:1	0.4	0.4	0.4	0.4	0.4
C22:0	0.2	0.2	0.2	0.2	0.2
C = C _{conv} (%) ^b		30.3	30.8	30.8	31.3

Experimental conditions: T = 160 °C, P = 0.16 MPa, catalyst loading: 0.05 wt % relative to amount of soybean oil

^a Sum of ct, tc and tt

^b conversion: $C = C_{\text{conv}} (\%) = [(IV_0 - IV_t)/IV_0] \times 100$

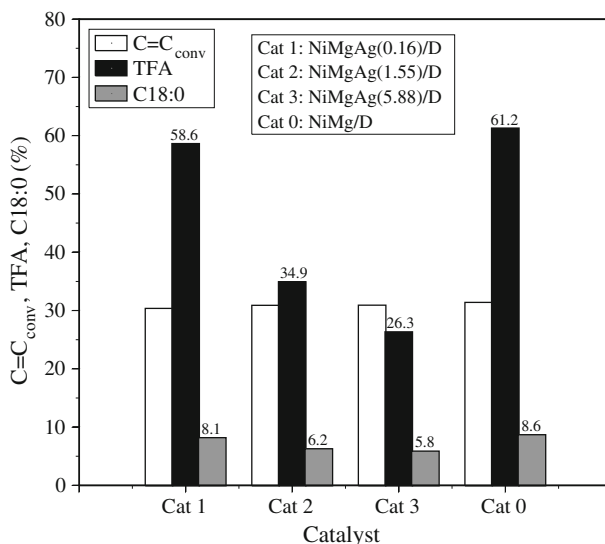


Fig. 6 Hydrogenation of soybean oil: TFA formation and stearic acid at C = C_{conv} = 30.8 ± 0.5

Hernandez [6], pores of small diameter favor the saturation of the fatty acid, since the successive hydrogenation is facilitated by the difficulty in the mobility of the bulky molecule. The results obtained clearly show that addition of silver to NiMg/D catalyst have significant effect on the distribution of CFA and TFA in hydrogenated oil.

The mechanisms of the hydrogenation and *cis*–*trans* isomerization are strongly interrelated. To describe the formation TFA an addition–elimination mechanism according to Horiuti-Polanyi is often assumed [48]. According to this mechanism, the selectivity of reaction is decided by the type of reaction of the half-hydrogenated intermediate: addition of the further chemisorbed hydrogen atom under hydrogenation to give less unsaturated fatty acid, in the case of catalysts with high affinity to hydrogen chemisorption, versus elimination of a hydrogen atom with TFA formation, in the case of weakly bonded hydrogen. Since hydrogenation is accompanied by isomerization, it can be proposed that the electron donor characteristic of the silver modified nickel catalyst would also affect this reaction. If the chemisorbed intermediate is removed quickly enough, it may not have time to isomerize to *trans* or in the case of linoleic acid, when hydrogenation of one of the double bonds is complete, the fatty acid molecule is released before hydrogenation of the second double bond can occur. The modification of the electronic properties and the presence of the geometric effect may both be used to explain the limited formation of C18:1*t* over silver modified NiMgAg/D catalysts compared to that of the NiMg/D catalyst. The beneficial effect of the silver addition to NiMg/D catalyst for the hydrogenation of soybean oil is observed for all of the catalysts tested in this work when considering the reduced TFA formation.

Kinetics of the hydrogenation of soybean oil

To describe the kinetics of both the hydrogenation and the *cis*–*trans* isomerization simplified kinetic model was assumed (Fig. 7), using first order rate equations with respect to the compositions of the various fatty acids in *cis* and *trans* configurations in the hydrogenated soybean oil.

In this model, the fatty acids are divided into five types: (a) C18:2*c*, linoleic acid, (*cis* configuration); (b) C18:2*t*, linoleic acid, (*trans* configuration); (c) C18:1*c*, oleic acid; (d) C18:1*t*, elaidic acid; (e) C18:0, stearic acid. Mathematical equations were developed for the proposed model for C18:2*c*, C18:2*t*, C18:1*c*, C18:1*t* and C18:0 as a function of time (*t*) based on the assumption that each of the 8 reaction steps shown (Fig. 7) follows first order kinetics based on the total amount of that types in the soybean oil. The k_i 's (k_1 – k_8) are the respective first order reaction rate constants.

Fig. 7 Simplified kinetic model for hydrogenation of soybean oil

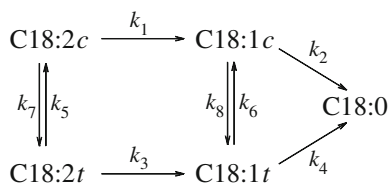


Table 7 Fitted kinetic parameters values for the studied catalysts at 160 °C and 0.16 MPa

Catalyst	k_1^a	k_2^a	k_3^a	k_4^a	k_5^a	k_6^a	k_7^a	k_8^a
NiMg/D	1.0×10^{-2}	3.0×10^{-4}	1.0×10^{-2}	3.5×10^{-4}	1.5×10^{-3}	2.5×10^{-3}	1.5×10^{-3}	1.5×10^{-2}
NiMgAg(0.16)/D	0.9×10^{-2}	5.6×10^{-4}	6.0×10^{-3}	6.0×10^{-5}	6.0×10^{-4}	2.0×10^{-3}	9.0×10^{-3}	1.0×10^{-2}
NiMgAg(1.55)/D	0.2×10^{-2}	3.0×10^{-4}	0.7×10^{-3}	2.5×10^{-5}	0.1×10^{-4}	0.9×10^{-3}	3.0×10^{-3}	4.0×10^{-3}
NiMgAg(5.88)/D	0.1×10^{-2}	2.0×10^{-4}	0.4×10^{-3}	2.0×10^{-5}	0.1×10^{-4}	0.1×10^{-3}	1.5×10^{-3}	2.0×10^{-3}

^a k_1 – k_8 denotes the first order kinetic rate constants in min^{-1}

The set of ordinary differential equations corresponding to the proposed model with mass action kinetics was solved numerically by the Gear algorithm [49]. The rate constants were obtained from kinetic runs by minimizing the sums of squares for deviations between the calculated and experimental concentrations of studying fatty acids. The minimization was performed by the simplex method [50].

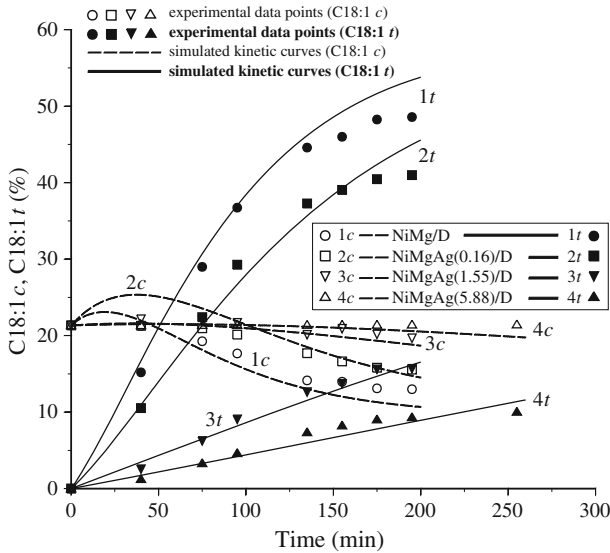


Fig. 8 Measured and simulated C18:1c and C18:1t versus reaction time

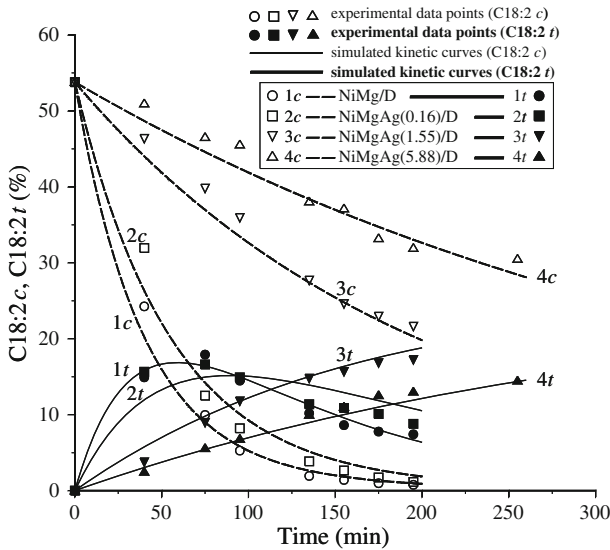


Fig. 9 Measured and simulated C18:2c and C18:2t versus reaction time

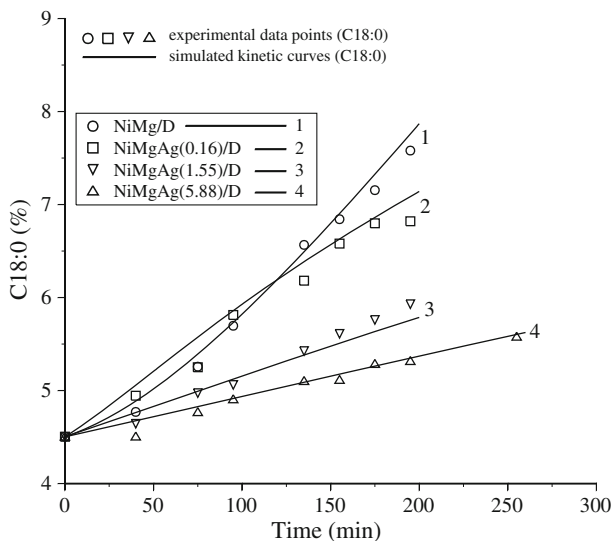


Fig. 10 Measured and simulated C18:0 versus reaction time

Table 7 establishes a comparison between the estimated rate constants for the hydrogenation of soybean oil over the studied catalysts.

From the table presented above, it can be noticed that the estimated isomerization rate constants k_7 and k_8 , and the estimated saturation constant k_3 , corresponding to the stearic acid formation, are higher in the case of NiMg/D and NiMgAg(0.16)/D catalysts. These observations are in agreement with experimental results, shown in Table 6 relating to the formed C18:1 t and C18:0 during the hydrogenation of soybean oil.

Figs. 8, 9 and 10 show a comparison between experimentally measured and simulated kinetics curves. As can be observed from Figs. 8, 9 and 10, the accuracy of the data for the simulations of concentration fatty acid profiles is quite satisfactory, with a relatively small deviation from the values obtained by experimental measurements.

In general, the simplified kinetic scheme, proposed to describe kinetics of soybean oil hydrogenation, gave a good description of the experimental data. The proposed kinetic model in Fig. 7 could be applicable for the hydrogenation of soybean oil under the studied operating conditions.

Conclusion

The effect of silver modifiers on the surface characteristics and catalytic behavior of NiMgAg/D catalyst was studied. Silver addition significantly affected reduction ability of modified catalysts. Larger nickel crystallites in the silver modified NiMg/D catalysts displayed easier nickel reduction than smaller nickel crystallites in the NiMg/D catalyst.

The NiMgAg/D catalysts had a lower selectivity towards TFA formation, and lower selectivity towards formation of stearic acid. The addition of silver inhibits hydrogenation activity, this effect being more obvious as the Ag loading is higher. The hydrogenation activity decreases in the following order: NiMg/D \geq NiMgAg(0.16)/D > NiMgAg(1.55)/D > NiMgAg(5.88)/D. The activity of catalysts was correlated with their available nickel surface area.

The estimated rate constants for soybean oil hydrogenation over studied catalysts obtained from the proposed simplified kinetic model showed good agreement with experimental results.

Acknowledgments This work was supported by the Ministry of Education, Science and Technological Development of the Republic of Serbia (Projects Nos. III 45001 and ON 172015).

References

1. O'Brien RD (2004) Fats and oils: formulating and processing for applications, 2nd edn. CRC Press, LLC, Boca Raton
2. Allen RR, Covey JE (1970) The effects of process variables on the formation of *trans*-unsaturation during hydrogenation. *J Am Oil Chem Soc* 47:494–496
3. Niklasson C, Andersson B, Schöön NH (1987) Influence of hydrogen pressure on selectivity in consecutive hydrogenation reactions. *Ind Eng Chem Res* 26:1459–1463
4. Makarvan IA, Matveeva OV, Davydova GI, Savchenko VI (2000) Lowering the *trans*-isomer content in hydrogenation of triglycerides of unsaturated fatty acids at ambient temperatures. *Stud Surf Sci Catal* 130:2039–2044
5. List GR, Neff WE, Holliday RL, King JW, Holser R (2000) Hydrogenation of soybean oil triglycerides: effect of pressure on selectivity. *J Am Oil Chem Soc* 77:311–314
6. Balakos MW, Hernandez EE (1997) Catalyst characteristics and performance in edible oil hydrogenation. *Catal Today* 35:415–425
7. Mikhailenko SD, Khlystov AS, Maksimova NA, Fasman AB (1983) Structural studies of nickel-based Raney catalysts. *React Kinet Catal Lett* 23:25–28
8. Stender S, Dyerber J (2004) Influence of *trans* fatty acids on health. *Nutr Metab* 48:61–66
9. Tarrago-Trani MT, Phillips KM, Lemar LE, Holden JM (2006) New and existing oils and fats used in products with reduced *trans*-fatty acid content. *J Am Diet Assoc* 106:867–880
10. Wright AJ, Wong A, Diosady LL (2003) Ni catalysts promotion of a *cis*-selective Pd catalyst for canola oil hydrogenation. *Food Res Int* 36:1069–1072
11. Belkacemi K, Boulmerka A, Arul J, Hamoudi S (2006) Hydrogenation of vegetable oils with minimum *trans* and saturated fatty acid formation over a new generation of Pd-catalyst. *Top Catal* 37:113–120
12. Li T, Zhang W, Lee RZ, Zhong Q (2009) Nickel-boron alloy catalysts reduce the formation of *trans* fatty acids in hydrogenated soybean oil. *Food Chem* 114:447–452
13. Stanković M, Gabrovska M, Krstić J, Tzvetkov P, Shopaska M, Tsacheva T, Banković P, Edreva-Kardjieva R, Jovanović D (2009) Effect of silver modification on structure and catalytic performance of Ni-Mg/diatomite catalysts for edible oil hydrogenation. *J Mol Catal A: Chem* 297:54–62
14. Alshaibani AM, Yaakob Z, Alsobaai AM, Sahri MQ (2012) Palladium-boron catalyst for vegetable oils hydrogenation. *Rasayan J Chem* 5:463–467
15. McArdle S, Leahy JJ, Curtin T, Tanner D (2014) Hydrogenation of sunflower oil over Pt–Ni bimetallic supported catalysts: preparation, characterization and catalytic activity. *Appl Catal A* 474:78–86
16. Martin GA, Mirodatos C, Praliand H (1981) Chemistry of silica-supported catalysts: preparation, activation and reduction. *Appl Catal* 1:367–382
17. Fernández MB, Piqueras CM, Tonneto GM, Crapiste G, Damiani DE (2005) Hydrogenation of edible oils over Pd-Me/Al₂O₃ catalysts (Me=Mo, V and Pb). *J Mol Catal A: Chem* 233:133–139

18. Gabrovska M, Krstić J, Tzvetkov P, Tenchev K, Shopska M, Vukelić N, Jovanović D (2011) Effect of the support and the reduction temperature on the formation of metallic nickel phase in Ni/silica gel precursors of vegetable oil hydrogenation catalysts. *Russ J Phys Chem A* 85:2392–2398
19. Chen AH, McIntire DD, Allen RR (1981) Modeling of reaction rate constants and selectivities in soybean oil hydrogenation. *J Am Oil Chem Soc* 58:816–818
20. Jovanović D, Čupić Ž, Stanković M, Rožić L, Marković B (2000) The influence of the isomerization reactions on the soybean oil hydrogenation process. *J Mol Catal A: Chem* 159:353–357
21. Belkacemi K, Boulmerka A, Hamoudi S, Arul J (2005) Activity and selectivity of novel structured Pd-catalysts: kinetics modeling of vegetable oils hydrogenation. *Int J Chem Reactor Eng* 3(A59):1–25
22. Albright LF, Allen RR, Moore MC (1970) Quantitative measure of geometrical isomerization during the partial hydrogenation of triglyceride oils. *J Am Oil Chem Soc* 47:295–298
23. Gabrovska M, Krstić J, Edreva-Kardjieva R, Stanković M, Jovanović D (2006) The influence of the support on the properties of nickel catalysts for edible oil hydrogenation. *Appl Catal A* 299:73–83
24. Kibby CL, Massoth FE, Swift HE (1976) Surface properties of hydrogen-reduced nickel chrysotiles. *J Catal* 42:350–359
25. Bartholomew CH, Pannell RB (1980) The stoichiometry of hydrogen and carbon monoxide chemisorption on alumina- and silica-supported nickel. *J Catal* 65:390–401
26. Hoang-Van C, Kachaya Y, Teichner SJ, Arnaud Y, Dalmon JA (1989) Characterization of nickel catalysts by chemisorption techniques, X-ray diffraction and magnetic measurements Effects of support, precursor and hydrogen pretreatment. *Appl Catal* 46:281–296
27. Bartholomew CH (1990) Hydrogen adsorption on supported cobalt, iron and nickel. *Catal Lett* 7:27–52
28. Coenen JWE, Linsen BG (1970) In: Linsen BG, Fortuin JMH, Okkerse C, Steggerda JJ (eds) Physical and chemical aspects of adsorbents and catalysts. Academic Press, London
29. IUPAC (1992) In: Diefenbacher A, Pocklington WD (eds) Standard methods for the analysis of oils, fats and derivatives, 7th edn 1st Supplement (Section 2, 2.001). Oxford, Blackwell, London
30. Lanje AS, Sharma SJ, Pode RB (2010) Synthesis of silver nanoparticles: a safer alternative to conventional antimicrobial and antibacterial agents. *J Chem Pharm Res* 2:478–483
31. Selim MM, El-Maksoud IHA (2005) Spectroscopic and catalytic characterization of Ni nano-size catalyst for edible oil hydrogenation. *Microporous Mesoporous Mater* 85:273–278
32. Gregg SJ, Sing KSW (1982) Surface area, and porosity, 2nd edn. Academic Press, London
33. Lowell S, Shields JE (1991) Powder surface area and porosity, 3rd edn. Chapman & Hall, London
34. Ghuge KD, Bhat AN, Babu GP (1993) Identification of nickel species and their interaction with the support in Ni–silica catalyst precursor. *Appl Catal A* 103:183–204
35. Montes M, de Bosscheyde P, Hodnett BK, Delannay F, Grange P, Delmon B (1984) Influence of metal-support interactions on the dispersion, distribution, reducibility and catalytic activity of Ni/SiO₂ catalysts. *Appl Catal* 12:309–330
36. Echeverria SM, Andres VM (1990) Effect of the method of preparation on the activity of nickel-Kieselguhr catalyst for vegetable oil hydrogenation. *Appl Catal* 66:73–90
37. Burattin P, Che M, Louis C (1997) Characterization of the Ni(II) phase formed on silica upon deposition–precipitation. *J Phys Chem B* 101:7060–7074
38. Mustard DG, Bartholomew CH (1981) Determination of metal crystallite size and morphology in supported nickel catalysts. *J Catal* 67:186–206
39. Bartholomew CH (1988) In: Paál Z, Menon PG (eds) Hydrogen effects in catalysis, fundamental and practical applications. Marcel Dekker, New York
40. Kumar N, King TS, Vigil RD (2000) A portal model for structure sensitive hydrogen adsorption on Ru–Ag/SiO₂ catalysts. *Chem Eng Sci* 55:4973–4979
41. Turlier P, Praliard H, Moral P, Martin GA, Dalmon JA (1985) Influence of the nature of the support on the reducibility and catalytic properties of nickel: evidence for a new type of metal support interaction. *Appl Catal* 19:287–300
42. Burattin P, Che M, Louis C (1999) Metal particle size in Ni/SiO₂ materials prepared by deposition–precipitation: influence of the nature of the Ni(II) phase and of its interaction with the support. *J Phys Chem B* 103:6171–6178
43. Roman A, Delmon B (1973) Promoter and carrier effects in the reduction of NiO/SiO₂. *J Catal* 30:333–342
44. Richardson JT, Turk B, Lei M, Forster K (1992) Effects of promoter oxides on the reduction of nickel oxide. *Appl Catal A* 83:87–101

45. Choi S, Ghim YS, Chang HN, Rhee JS (1986) Hydrogenation of soybean oil by nickel/silica catalysts in a rotating packed disk reactor. *J Am Oil Chem Soc* 63:1351–1355
46. Lefèbvre VJ, Baltes J (1975) Nickel/silber-hydrierkatalysatoren und ihre verwendung zur selektiven härtung von fetten. *Fete Seifen Anstrichmittel* 77:125–131
47. Macher M (2001) Supercritical hydrogenation of vegetable oils. PhD thesis, Chalmers University of Technology, Göteborg, Suecia
48. Horiuti I, Polanyi M (1934) Exchange reactions of hydrogen on metallic catalysts. *Trans Faraday Soc* 30:1164–1172
49. Gear CW (1971) Numerical initial value problems in ordinary differential equations. Prentice Hall, Englewood Cliffs
50. Stone RE, Tovey CA (1991) The simplex and projective scaling algorithms as iteratively reweighted least squares methods. *SIAM Rev* 33:220–237